PHYSICAL REVIEW B **86**, 024506 (2012)

Decay of persistent precessing domains in ^{3}He-B at very low temperatures

S. N. Fisher,[1] G. R. Pickett,[1] P. Skyba,[1,2] and N. Suramlishvili[3]

[1]*Department of Physics, Lancaster University, Lancaster, LA1 4YB, United Kingdom*

[2]*Center of Low Temperature Physics, Institute of Experimental Physics, Slovak Academy of Sciences, Watsonova 47, 04001 Košice, Slovakia*

[3]*School of Mathematics and Statistics, Newcastle University, Newcastle NE1 7RU, United Kingdom (also Andronikashvili Institute of Physics, Tbilisi, 0177, Georgia)*

(Received 23 May 2012; published 6 July 2012)

The B phase of superfluid ^{3}He can support regions of extremely long-lived coherent spin precession at ultralow temperatures, known as persistent precessing domains (PPD). The domains have been described in terms of a Bose-Einstein condensate of magnons and in terms of Q balls in field theory. The domains form in a magnetic field minimum along the vertical axis of a cylindrical cell. When far from the ends of the cell, the PPD lifetime grows exponentially on decreasing temperature. When the PPD is close to the horizontal end wall of the cell, an extra surface dissipation mechanism dominates at low temperatures. We present measurements of the PPD generated at various locations in the cell over a broad range of temperatures below 0.3 T_C. We compare the measured properties with theoretical expectations for spin-wave modes. We present model calculations of different dissipation mechanisms and we compare these to the measured lifetimes.

DOI: 10.1103/PhysRevB.86.024506 PACS number(s): 67.30.er, 67.30.hj, 76.60.−k

I. INTRODUCTION

In zero magnetic field, the B phase of superfluid ^{3}He has an isotropic energy gap and there is no nett spin or orbital angular momentum. However, in an applied field the Cooper pairs, which form the superfluid condensate, become polarized resulting in a nett spin **S** and an orbital angular momentum **L**. The spin and orbital degrees of freedom are coupled by the spin-orbit "dipole" interaction. Spin dynamics are readily probed by NMR experiments. To date, most NMR experiments have been performed at relatively high temperatures where the orbital momentum is heavily damped by the normal fluid component. In this case, the resulting spin dynamics are well described by the celebrated Leggett equations.[1] Long-range coherence of the spin degrees of freedom gives rise to spin supercurrents which can redistribute the spin (magnetization) throughout the experimental volume. At very low temperatures, the dynamics of the orbital angular momentum may also play an important role.[2,3]

The spectacular effects of spin supercurrents in the B phase are demonstrated at relatively high temperatures by the long-lived mode of coherent spin precession known as the homogenously precessing domain (HPD).[2,4,5] The formation and stability of the HPD is essentially governed by the spin stiffness of the order parameter and by spin-orbit coupling. Spin supercurrents provide feedback which acts on the spin-orbit coupling to stabilize coherent spin precession even in very inhomogeneous magnetic fields.[6] In this sense, superfluid ^{3}He may be considered as a spin (magnetic) superfluid. Indeed, the HPD has been described in terms of a Bose-Einstein condensate of magnons.[7,8]

The intrinsic decay mechanism of the HPD is provided by Leggett-Takagi relaxation[9] which couples the spins of the normal fluid and superfluid components. As the normal fluid component decreases towards lower temperatures, the HPD lifetime grows. At very low temperatures, the density of thermal excitations falls exponentially so one might expect an exponential increase in the lifetime. However, the HPD becomes unstable at temperatures below $\sim 0.4T_c$ and decays quickly at lower temperatures.[10] Owing to spin-orbit coupling, the spatial distribution of the orbital angular momentum direction (the texture) is significantly modified by the HPD.[6,11,12] Furthermore, at low temperatures, the damping is sufficiently small to allow oscillations in the texture which can destabilize the HPD.[13–15]

In the low-temperature limit, an extremely long-lived NMR signal was observed in Lancaster.[16] This was first called the persistent induction signal (PIS). It is now commonly referred to as the persistent precessing domain (PPD), but is also sometimes called a Q ball.[7,17] Remarkably, the free decay of the PPD may exceed half an hour at the lowest temperatures.[18]

Early experiments revealed several other remarkable properties of the PPD. First it was found that, unlike HPD, the frequency of the PPD increases during its decay.[16] The PPD was first generated by pulsed NMR, but in contrast to HPD, it only required small tipping pulses, of the order of a few degrees.[16] The PPD could also be generated by continuous excitation, but not by conventional cw NMR. Instead, the PPD required a new technique, named off-resonant cw NMR.[19] Here the continuous excitation is supplied at a *different* frequency to the signal. The PPD was only excited if the excitation frequency was higher than the signal frequency.[19] Astonishingly, it was found that the PPD could even be excited by applying white noise to the excitation coil.[20] These latter properties give a remarkable demonstration of spin superfluidity and, perhaps, give the strongest indications that the PPD can be considered as a Bose-Einstein condensate of magnons, as was suggested by Bunkov and Volovik.[7]

Experiments show very clearly that the free decay of the PPD is independent of the method of excitation.[19] However, in early experiments[16] the properties of the PPDs showed a broad variation even under nominally identical external conditions. The PPD was highly irreproducible, and was only occasionally excited by pulsed NMR. This shows that the texture plays an important role. Later experiments, using a cylindrical cell along the field direction, revealed that under certain circumstances reproducible PPD signals could be generated.

Further experiments were performed using two NMR pick-up coils to give information on the spatial position of the PPD.[21] These confirmed earlier suspicions that the reproducible PPDs are generated in a field minimum along the cell axis.[22]

Recent experiments in Helsinki,[17,23] using a similar cell geometry, have shown that spin waves in the field minimum can be excited by conventional cw NMR at higher temperatures. The spin waves were found to become nonlinear at large spin deflection angles. Crucially, these experiments showed that the PPD can be identified as the ground-state mode which becomes very long lived at the lowest temperatures, whereas the higher modes become unstable at low temperatures and quickly decay into the ground-state mode.

Here we present detailed measurements of the PPD at different locations in the cell. We compare the measured properties with expectations for spin-wave modes and we discuss the dissipation mechanisms.

II. THE EXPERIMENTAL ARRANGEMENT

The experimental cell is shown in Fig. 1. The NMR chamber is formed by a vertical sapphire tube with inside diameter 4.3 mm. The tube is sealed at the top with a rounded sapphire end cap and open at the bottom to the inner cell of a Lancaster style nuclear cooling stage.[24,25] Surrounding this is an outer cell which acts as a thermal guard to reduce heat leaks. The cell is filled with liquid ^{3}He and attached to the Lancaster Advanced dilution refrigerator.[26] The lowest temperature achieved was $\sim 0.11 T_c$ as inferred from the vibrating wire resonator[27,28] situated below the sapphire tube.

NMR measurements are made using the two transverse pick-up coils shown in Fig. 1. Pick-up coil No. 1 is close to the rounded end of the NMR chamber, while pick-up coil No. 2 is located towards the middle of the sapphire tube. The two pick-up coils are located slightly above the center of the main solenoid (fixed to the still radiation shield of the refrigerator) which provides the ~60 mT vertical magnetic field for the NMR experiments. Consequently the magnetic field profile from the main solenoid is slightly curved in the region of the NMR chamber. In addition to the main solenoid

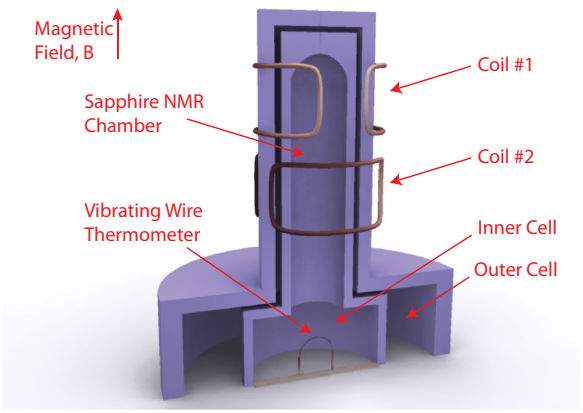

FIG. 1. (Color online) A schematic of the double walled experimental cell. Two saddle coils are used to excite and detect the PPD in different locations. The NMR chamber is formed by a cylindrical sapphire tube extending up from the inner cell.

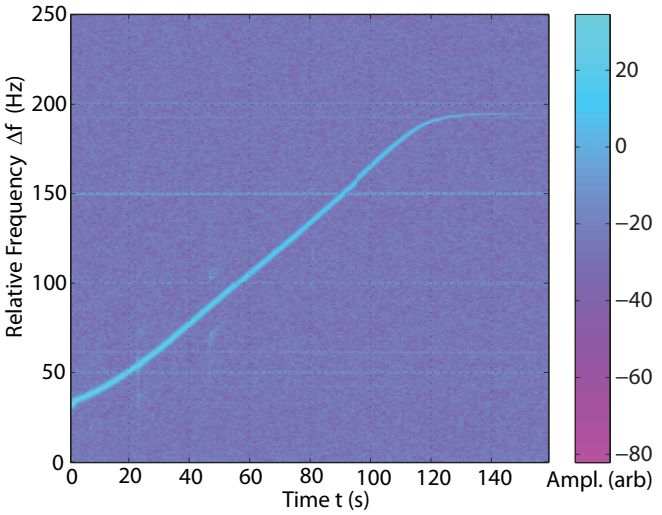

FIG. 2. (Color online) A typical PPD signal. The plot shows a time-dependent Fourier transform of the output signal from the mixer, giving the relative frequency Δf as a function of time. The color scale indicates the signal amplitude (see text).

is a field gradient coil (fixed to the 20-mK shield of the refrigerator) which provides a linear field gradient. With an appropriate combination of currents applied to the solenoids, a field minimum is generated along the axis of the NMR chamber and the position of the minimum is easily varied by changing the applied field gradient.

III. THE FREE DECAY OF PPDS

All of the measurements presented below were made using pulsed NMR at 0 bar pressure. The pulsed excitation was adjusted to give a tipping angle of around 15° to give the maximum PPD signal strength (the initial amplitude of the NMR signal is increased by having a larger tipping pulse, but this then very quickly decays to a smaller value which we associate with the long-lived PPD). The PPD signals are mixed with a reference frequency $f_{\rm ref}$ which can be fine tuned to suit the measurement but is always close to the Larmor frequency of around 1.25 MHz. The output from the mixer gives signal frequencies relative to the reference frequency, $\Delta f = |f - f_{\rm ref}|$. The low-frequency output signal is then analyzed by taking its Fourier transform as a function of time, giving information on both the signal strength and its (relative) frequency. Figure 2 shows an example of a PPD analyzed by this method. The Fourier transform is plotted in the frequency-time domain with a color scale to indicate the strength of the signal: The lighter areas in the plot indicate the higher signal strengths. The vertical axis gives the frequency Δf relative to the reference frequency which was chosen to be ~30 Hz below the initial frequency of the PPD. The absolute value of the signal frequency is easily determined by varying the reference signal.

IV. SPATIAL DEPENDENCE OF FREELY DECAYING PPDS

In Fig. 3 we plot the lifetime of the PPD, measured with coil No. 1, as a function of the current applied to the field gradient coil. The measurements were made at the base temperature

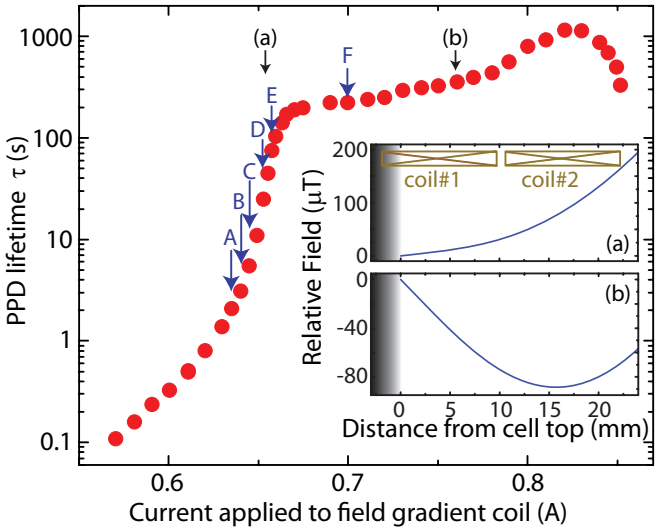

FIG. 3. (Color online) The lifetime of the PPD as a function of the current applied to the field gradient coil. The measurements were taken using coil No. 1. The inset shows calculated field profiles at two different applied field gradients, showing that the field minimum is well within the cell at (b) and moves out of the cell as the gradient falls below the value indicated at (a). The labels A, B, C, D, E, and F indicate the applied field gradients at which further measurements are presented in Figs. 4–6.

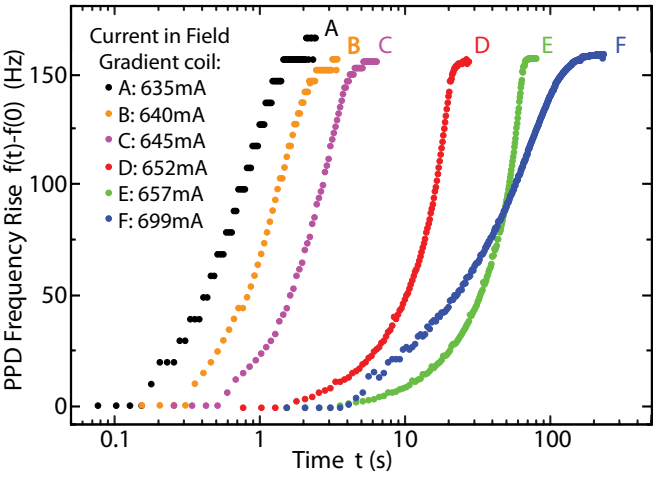

FIG. 4. (Color online) The increase in the frequency of the PPD as a function of time during its free decay. The curves A, B, C, D, E, and F correspond to different applied field gradients as indicated in Fig. 3.

of the cell, $T \simeq 0.11 T_C$. The signal amplitudes do not decay exponentially (see below) so we define the lifetime to be the time over which the PPD signal can be observed in the time-dependent Fourier transform (an example of which is shown in Fig. 2).

For the larger gradients in Fig. 3, the field minimum is far from the top of the cell, and the PPD is located below coil No. 1 (in this case the signal amplitude is larger in coil No. 2). The signal amplitude falls quickly as the PPD is moved outside of the pick-up coil. So the apparent decrease in the PPD lifetime measured by coil No. 1 at the largest field gradients (for currents above 0.83 A in Fig. 3) is an artifact of the smaller signal amplitude (the weaker signals disappear into the noise level earlier). On decreasing the field gradient, the location of the field minimum and the PPD moves up towards the top of the cell. The lifetime of the PPD first shows a gradual decrease as the PPD is moved towards the top of the cell. On further decreasing the applied field gradient, the field minimum moves past the top of the cell and the PPD is "pushed" up against the top wall of the chamber. Now we see a very dramatic decrease in the PPD lifetime which clearly indicates the presence of an additional "surface" dissipation mechanism.

V. PROPERTIES OF THE FREELY DECAYING PPDS

The frequency rise of the PPD, $f(t) - f(0)$, as a function of time during its decay is shown in Fig. 4. The frequency is obtained from the Fourier transform of the signal. Six different decays are shown corresponding to different applied field gradients. The applied field gradients used are indicated by labels A–F in Fig. 3. The shortest lived PPD signal, labeled A in the figure, corresponds to the smallest applied field gradient, where the field minimum is furthest above the top of the cell. The longest lived PPD signal, labeled F in the figure, corresponds to the largest applied field gradient, where the field minimum is now located within the experimental cell. The total change in frequency during the PPD decay is seen to be very similar in all cases despite the large variation in the lifetime. Note that the frequency is almost constant at the end of the PPD decay, which is also evident in Fig. 2.

The amplitude of the PPD as a function of time during its decay is shown in Fig. 5. The vertical axis shows the voltage amplitude of the output signal from the mixer. The signal amplitude can also be obtained from the Fourier transform of the signal, but the noise is much higher in this case. The six curves shown correspond to the same PPD signals plotted in Fig. 4. For each curve, the data points end at the point where the signal is no longer visible on the Fourier transform (note that the PPD remains visible in the Fourier transform well after the direct signal voltage has bottomed out at the noise level).

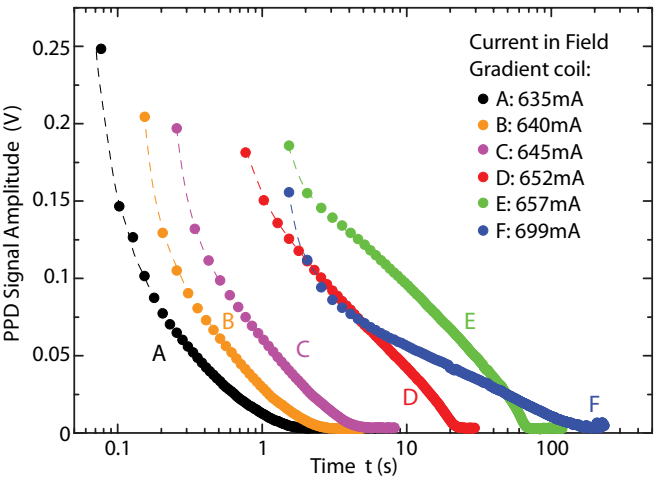

FIG. 5. (Color online) The amplitude of the PPD signal, measured directly from the voltage data, as a function of time during its decay. The data show the same PPDs used in Fig. 4.

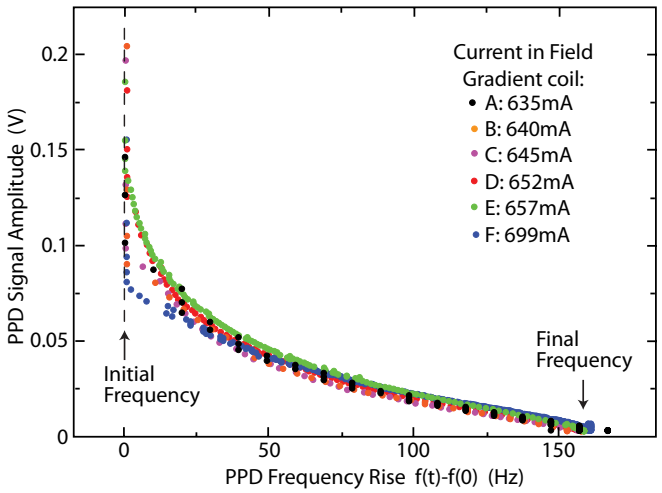

FIG. 6. (Color online) The amplitude of the PPD signal as a function of its rise in frequency, $f(t) - f(0)$. The data show the same PPDs used in Figs. 4 and 5.

In Fig. 6 we plot the amplitude of the PPD signal against its frequency rise, again for the same six PPDs shown in Figs. 4 and 5. The data collapse very accurately onto a single curve, particularly at later times (smaller amplitudes). So the dependence of the signal amplitude on the frequency shift is an intrinsic property of the PPD, independent of the dissipation rate.

VI. LINEAR SPIN WAVES IN A COMBINED FIELD-TEXTURE POTENTIAL WELL

Here we present a theory for small amplitude spin waves excited along the axis of a flare-out texture in the presence of a shallow axial field minimum. In subsequent sections, we will compare the predictions of this theory to the measurements of the PPD.

The role of the field minimum was investigated theoretically by Kupka and Skyba.[29] They considered a one-dimensional model a uniform l texture parallel to the magnetic field. They found a solution in which the spin precesses coherently in a parabolic field minimum. For a shallow field minimum, $\nabla^2\omega_L \ll \omega_L^3/c_L^2$, a series of modes were found corresponding to spin waves excited along the field axis.

Along the radial direction of the cylindrical cell, spin-wave modes can also form in the potential provided by the spatially varying texture as was studied in detail by Bunkov and Volovik[7] and later by Eltsov *et al.*[23]

Below, we derive expressions for spin-wave modes in three dimensions for a cylindrical cell along the vertical z axis. The cell is assumed to have a static flare-out texture in which the orbital momentum is aligned along the field direction along the cell axis, and smoothly deflects along the radial direction to be perpendicular to the vertical cell walls. Close to the cell axis, the flare-out texture produces a parabolic potential for spin waves in the radial direction and the field minimum provides a parabolic potential along the axial direction.

The B-phase order parameter is characterized by a matrix describing relative rotations of spin and orbital spaces. Usually the orbital degrees of motion are assumed to be frozen by orbital viscosity. This approach is clearly valid at high temperatures, but orbital viscosity decreases exponentially at very low temperatures[30] and the resulting spin-orbit dynamics become very complex.[3] In the following we neglect orbital dynamics but we will return to this issue in Sec. XI.

The order parameter can be written in terms of three Euler angles: α, β, and γ. The angle γ describes rotations around the spin direction, β gives the deflection of the spin from the vertical axis, and α is the azimuthal angle. In Cartesian coordinates the spin is given by

$$\begin{aligned} S_x &= \frac{\chi}{g^2}\omega_p \cos\alpha \sin\beta, \\ S_y &= \frac{\chi}{g^2}\omega_p \sin\alpha \sin\beta, \\ S_z &= \frac{\chi}{g^2}\omega_p \cos\beta, \end{aligned} \tag{1}$$

where χ is the susceptibility and $g \approx 2 \times 10^8$ rads^{-1}T^{-1} is the gyromagnetic ratio of ^{3}He. It is often useful to define a fourth angle $\phi = \alpha + \beta$. To describe spin waves, we start with the Lagrangian function introduced in Ref. 29, generalized for the three dimensions. We search for the stationary spin-wave solutions of the form,

$$\begin{aligned} &\dot\alpha = -\omega_p, \quad \dot\phi = 0, \quad \dot\beta = 0, \\ &\nabla\alpha = \nabla\phi = 0, \end{aligned} \tag{2}$$

where ω_p is the spin precession frequency.

Following the approach developed by Kupka and Skyba,[29] we assume a parabolic field minimum which we can express in terms of the local Larmor frequency,

$$\omega_L(z) = gB(z) = \omega_0 + z^2\nabla^2\omega_L, \tag{3}$$

where ω_0 is the Larmor frequency at the field minimum. The potential due to the orbital texture in the radial direction is determined by the dipole potential, which for small spin deflections can be written as[23,31]

$$E_{\rm dip} = 4\frac{\chi_B}{\gamma^2}\Omega^2\left(\frac{2}{5}\sin^2\frac{\beta_l}{2}\sin^2\frac{\beta}{2} - \sin^4\frac{\beta_l}{2}\sin^4\frac{\beta}{2}\right), \tag{4}$$

where β_l is the angle between the orbital momentum vector and the z axis and Ω is the Leggett frequency for the B phase. In the flare-out texture, the angle β_l varies linearly with radial distance r close to the axis of the cell. So close to the axis of the cell, β_l is small and can be written as $\beta_l = \beta_l' r$, where $\beta_l' = \partial\beta_l/\partial r$ is the gradient of the orbital deflection angle close to the cell axis.

For these conditions, the Lagrangian function reduces to

$$L = -\frac{1}{2}\frac{\chi_B}{\gamma^2}c_{||}^2(\nabla\beta)^2 + \frac{1}{2}\frac{\chi_B}{\gamma^2}\omega_p(\omega_p - \omega_L(z))\beta^2 - E_{\rm dip}, \tag{5}$$

and the corresponding Lagrange equation is

$$\frac{d}{dt}\frac{\partial L}{\partial\dot\beta} + \frac{\partial}{\partial\mathbf{r}}\frac{\partial L}{\partial\nabla\beta} - \frac{\partial L}{\partial\beta} = 0. \tag{6}$$

Using the conditions specified above, and assuming the spin deflection β is small, the Lagrange equation can be written explicitly in cylindrical coordinates (r,φ,z) as

$$-c_{||}\nabla^2\beta + \omega_p\nabla^2\omega_L z^2\beta + \tfrac{4}{5}\Omega^2\beta_l'^2 r^2\beta - \omega_p(\omega_p - \omega_0)\beta = 0. \tag{7}$$

The solution of this equation can be written as

$$\beta = \beta_0 \psi(z)\theta(r,\varphi), \tag{8}$$

representing a product of axial and radial harmonic oscillator solutions.

The axial component $\psi(z)$ is a solution to the axial part of Eq. (7):

$$-\frac{d^2\psi}{dz^2} + \frac{\omega_p \nabla^2 \omega_L}{c_{||}^2} z^2 \psi = \frac{\omega_p(\omega_p - \omega_0)}{c_{||}^2}\psi. \tag{9}$$

The normalized solution is

$$\psi_n(z) = \left(\frac{1}{2^n n! \pi^{1/2} Z}\right)^{1/2} H_n\left(\frac{z}{Z}\right)\exp\left(-\frac{z^2}{2Z^2}\right), \tag{10}$$

where n is an integer and the axial extent of the spin wave is characterized by

$$Z = \left(\frac{c_{||}^2}{\omega_0 \nabla^2 \omega_L}\right)^{\frac{1}{4}}, \tag{11}$$

where H_n is the nth order Hankel function. This corresponds exactly to the solution derived in Ref. 29. The frequency shift associated with the axial mode is

$$\delta\omega_z = \delta\omega_z^0(2n+1), \tag{12}$$

where

$$\delta\omega_z^0 = c_{||}\sqrt{\frac{\nabla^2\omega_L}{\omega_0}}. \tag{13}$$

The radial component describes a two-dimensional oscillator which obeys the radial part of Eq. (7):

$$-\frac{\partial^2\theta}{\partial r^2} - \frac{1}{r}\frac{\partial\theta}{\partial r} - \frac{1}{r^2}\frac{\partial^2\theta}{\partial\varphi^2} + \frac{4}{5}\frac{\Omega^2}{c_{||}^2}\beta_l'^2 r^2\theta = \frac{\omega_p(\omega_p-\omega_0)}{c_{||}^2}\theta. \tag{14}$$

The normalized solution is

$$\theta(r,\varphi) = \sqrt{\frac{k!}{\pi\Gamma(k+l+1)}}\frac{r^l}{R^{l+1}}L_k^l\left(\frac{r^2}{R^2}\right) \times \exp\left(\frac{r^2}{2R^2}\right)\exp(\pm il\varphi), \tag{15}$$

where k and l are positive integers (quantum numbers), $\Gamma(k+l+1)$ is the gamma function, $L_k^l(r^2/R^2)$ is the generalized Laguerre polynomial, and the radial extent of the spin-wave mode is characterized by

$$R = \left(\frac{5}{4}\right)^{1/4}\sqrt{\frac{c_{||}}{\beta_l'\Omega}}. \tag{16}$$

The corresponding frequency shift is

$$\delta\omega_r = \delta\omega_r^0(k+l+1), \tag{17}$$

where

$$\delta\omega_r^0 = \frac{4}{\sqrt{5}}\frac{\Omega}{\omega_0}c_{||}\beta_l'. \tag{18}$$

We note that this expression differs by a numerical prefactor of approximately 3 compared to the expression given in Ref. 23.

The total frequency shift of linear spin waves is given by the sum of the radial and axial shifts:

$$\delta\omega_{nkl} = \omega_p - \omega_0 = \delta\omega_z^0(2n+1) + \delta\omega_r^0(k+l+1). \tag{19}$$

VII. COMPARISON OF THE PPD WITH LINEAR SPIN-WAVE MODES

Recent experiments[17,23] clearly show that the PPD emerges from the fundamental spin-wave mode at low temperatures. However, the linear spin-wave theory given above is only applicable for small spin deflection angles, so we can only make a direct comparison to the late-time properties of the PPD, that is at the end of its decay where its amplitude tends to zero.

The fundamental spin-wave resonance, corresponding to the quantum numbers $n,k,l = 0$, is given by

$$\beta = \beta_0\exp\left(-\frac{z^2}{2Z^2}\right)\exp\left(-\frac{r^2}{2R^2}\right), \tag{20}$$

where β_0 is the spin deflection at the center of the PPD, and Z and R are given by Eqs. (11) and (16), respectively.

To make a quantitative comparison with experiments, we assume that the spin-wave velocity is given by[32]

$$c_{||} = v_F\sqrt{\frac{3}{10}\left(1+\frac{Z_0}{4}\right)}, \tag{21}$$

where Z_0 is the Fermi liquid parameter. At 0 bar pressure, $Z_0 = -2.69$ and $v_F = 59\ \mathrm{ms}^{-1}$,[33] giving a spin-wave velocity of $c_{||} = 18.5\ \mathrm{ms}^{-1}$. For our experimental conditions we estimate that $\beta_l' \sim \pi/D$, where $D = 4.3$ mm is the diameter of the cell, which is consistent with the simulations given in Ref. 17. From measurements of the spatial manipulation of the PPD[22] we estimate the field minimum to have $\nabla^2\omega_L \approx 2\pi \times 6\ \mathrm{MHzm}^{-2}$. The Leggett frequency at 0 bar pressure is $\Omega \approx 2\pi \times 100$ kHz[34] and ω_0 is approximately equal to the PPD frequency, $\omega_0 \approx 2\pi \times 1.25$ MHz. Inserting these parameters into Eqs. (11) and (16) gives the axial extent of the fundamental spin-wave mode to be $2Z \approx 2.1$ mm and the diameter is $2R \approx 0.42$ mm.

The total frequency shift of the fundamental spin-wave mode is

$$\delta\omega_{000} = \delta\omega_z^0 + \delta\omega_r^0. \tag{22}$$

Using the values estimated above for our experimental conditions, the axial contribution to the frequency shift is quite small, $\delta\omega_z^0/(2\pi) \approx 6.4$ Hz. The radial contribution is larger, $\delta\omega_r^0/2\pi \approx 308$ Hz (we note that the expression given in Ref. 23 gives a somewhat smaller value of $\delta\omega_r^0/2\pi \approx 93$ Hz). The total shift is thus expected to be $\delta\omega_{000}/2\pi \approx 314$ Hz, and is dominated by the radial contribution. This frequency shift is roughly twice as large as the time-dependent shifts observed in the PPD measurements shown in Fig. 4. This implies that the initial frequency shift of the PPD is roughly half of the shift predicted for linear spin waves.

VIII. NONLINEAR SPIN WAVES

The spin-wave modes described above are linear; the frequency shift does not depend on the spin deflection. In

contrast the PPD is clearly nonlinear with an amplitude dependent frequency shift, shown in Fig. 6. The spin-wave modes excited by conventional cw NMR at higher temperatures display similar nonlinearities.[7,23] The frequency increases with decreasing signal amplitude. The nonlinear response can be semiquantitatively understood by taking into account the "back-reaction" on the texture as formulated by Bunkov and Volovik.[7] For large spin deflection angles (large signal amplitudes), the l texture is flattened (β_l' is reduced) which reduces the frequency shift and increases the size of the precessing domain. As the signal decays the orbital texture relaxes back towards the equilibrium flare-out texture, the precessing domain shrinks, and the frequency increases.

The size of the PPD signal provides information on the spatial extent of the PPD and the deflection of its precessing spins. The initial size of the PPD signals is typically 1%–2% of the initial size of HPD signals which are observed in the same cell at higher temperatures. The HPD corresponds to the entire active region precessing coherently with $\beta = 104^\circ$. The volume of the active region within the NMR pick-up coils is $V \approx L_0 \pi D^2/4$ where $L_0 \approx 10$ mm is the length of the coils. The fraction of the active volume which is taken up by the ground-state linear spin-wave mode is thus $(2Z/L_0) \times (2R/D)^2 \approx 2 \times 10^{-3}$. This is roughly 10 times smaller that the initial PPD signal relative to the HPD. We therefore conclude that the initial size of the PPD must be considerably larger than the linear spin-wave mode described in the previous sections.

We can compare the amplitude-dependent frequency shift with estimates given in Ref. 7 for nonlinear spin waves. For low-amplitude spin waves of roughly equal radial and axial dimensions $Z \sim R$ the nonlinear frequency shift (the frequency shift from the linear spin-wave mode) was estimated to be[7]

$$\Delta\omega \sim -\frac{\Omega^3}{\omega_0}\frac{L_0}{c_{||}}\left(\frac{M_\perp}{M_{\rm HPD}}\right)^2, \qquad (23)$$

where $M_\perp$ is the strength of the spin-wave signal (the transverse magnetization) and $M_{\rm HPD}$ is the corresponding signal which would be measured if HPD filled the experimental cell. The magnitude of the nonlinear shift given by Eq. (23) is comparable to experimental observations of the PPD. However, in contrast to Eq. (23), the PPD frequency varies quite linearly with amplitude towards the end of its decay.

IX. TEMPERATURE DEPENDENCE OF FREELY DECAYING PPDS

The temperature dependence of the PPD lifetime is shown in Fig. 7. We define the lifetime to be the time after which the Fourier-transformed signal amplitude falls below the noise level. At higher applied field gradients, the field minimum is relatively far from the end of the cell and the PPD lifetime increases exponentially with decreasing temperature as the thermal quasiparticle excitation density is exponentially suppressed. As the applied field gradient is decreased, the field minimum moves closer to the end of the cell and the PPD lifetime tops out at low temperatures. The closer the field minimum to the top of the cell, the shorter the PPD lifetime at the lowest temperatures. Clearly the behavior suggests two distinct dissipation mechanisms. An intrinsic mechanism due

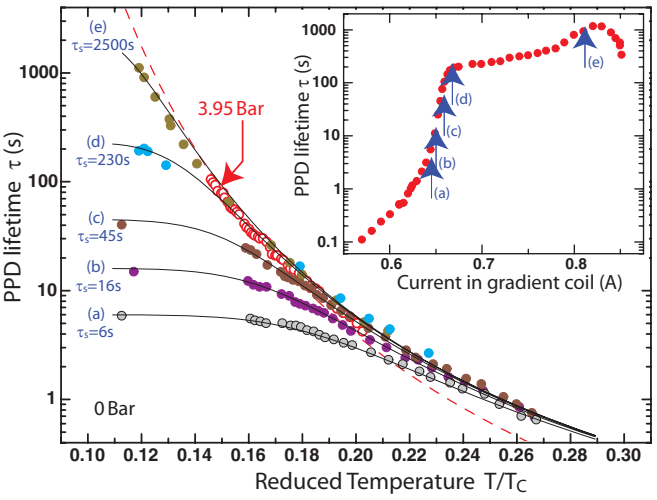

FIG. 7. (Color online) The lifetime of the PPD as a function of reduced temperature, T/T_C, for various applied field gradients. Data at 0 bar pressure are shown for five different applied field gradients, labeled (a)–(e) as indicated in the inset. The inset shows the lifetime at the lowest temperatures as a function of the current applied to the gradient coil. Open circles show data taken at 3.95 bar pressure for PPD held well away from the end of the cell. Lines give fits to the data using Eqs. (24) and (25) with different values for the surface relaxation lifetime τ_s as indicated. The dashed line corresponds to $3\tau_{\rm DF}$, where $\tau_{\rm DF}$ is given by Eq. (50); see text.

to thermal quasiparticles and an additional surface mechanism associated with the close proximity to the end wall of the cell. The surface mechanism is seen to be relatively temperature independent. Comparing with the single data set taken at 3.95 bar (open red circles in the figure) shows that the intrinsic mechanism is quite insensitive to pressure when plotted as a function of T/T_C.

To model the combined effects of intrinsic and surface relaxation mechanisms, we write the measured lifetime of the PPD as

$$\tau = \left(\tau_i^{-1} + \tau_s^{-1}\right)^{-1}, \qquad (24)$$

where τ_s is the surface limited lifetime which dominates at the lowest temperatures close the end wall of the container, and τ_i is the lifetime limited by intrinsic relaxation mechanism which dominates far from the end wall of the container. The solid lines in Fig. 7 show fits to the data with different values of τ_s for the different applied field gradients, as indicated. The lines have a common intrinsic lifetime given by

$$\tau_i = A\sqrt{\frac{k_B T}{\Delta_0}}\exp\left(\frac{\Delta_0}{k_B T}\right), \qquad (25)$$

where $A = 2.62 \times 10^{-3}$s is a fitting parameter adjusted to fit the data at higher temperatures and Δ_0 is the energy gap.

X. RELAXATION MECHANISMS AT LOW TEMPERATURES

Below we discuss some possible spin relaxation mechanisms in the low-temperature ballistic quasiparticle regime. In particular, we present model calculations of the lifetimes of the fundamental linear spin-wave modes according to

Leggett-Takagi and spin diffusion mechanisms, and we compare these with the measured lifetimes of the PPD. We also briefly discuss the surface relaxation.

The lifetime of the spin precession can be obtained by comparing the total energy of the precessing domain with the power dissipated, $\tau \sim E/(dE/dt)$. We can define the Hamiltonian as $H = E_V = \dot{\alpha}\frac{\partial L}{\partial \dot{\alpha}} - L$. The energy density within precessing domain is dominated by the energy required to deflect the spins from the field direction, so

$$E_V \approx \frac{1}{2}\frac{\chi_B}{\gamma^2}\dot{\alpha}_s^2\beta^2 \approx \frac{1}{2}\frac{\chi_B}{\gamma^2}{\omega_0}^2\beta^2. \tag{26}$$

The total energy of the fundamental spin-wave mode is the volume integral of the energy density:

$$E = \int E_V dV \approx \frac{\pi^{3/2}}{2} Z R^2 \frac{\chi_B}{\gamma^2}{\omega_0}^2{\beta_0}^2. \tag{27}$$

This gives the energy which is dissipated during the relaxation. In general, the energy dissipated can be written in terms of a dissipation function R_d as

$$\frac{dE}{dt} = -2\int R_d dV. \tag{28}$$

The dissipation function may have several components, $R_d = \sum_i R_i$, corresponding to different relaxation mechanisms. The corresponding decay time of the precessing structure can be written as $\tau = (\sum_i 1/\tau_i)^{-1}$. In the bulk superfluid, far from the container walls, there are two main mechanisms for dissipation which have been identified experimentally: Leggett-Takagi relaxation and spin diffusion.

To derive the corresponding dissipation functions, we use the methods developed by Markelov[35,36] for Leggett-Takagi relaxation and by Markelov and Mukharsky[37] for spin diffusion. We start with the nonlinear kinetic equation obtained by Combescot:[38]

$$\frac{\partial \delta\nu}{\partial t} + (\mathbf{v_F}\nabla)\delta\mu + \delta\mu \times \delta\mathbf{E} = -\frac{\delta\mu}{\tau_{\mathbf{qp}}}, \tag{29}$$

where

$$\delta\mu = \delta\nu - \frac{\partial\varphi}{\partial E}\delta\mathbf{E}, \tag{30}$$

$$\varphi = -\tanh\frac{E}{2k_BT}, \tag{31}$$

$$\delta\mathbf{E} = k_i\mathbf{A_i} + \frac{\xi}{\mathbf{E}}\mathbf{X} - \left(\mathbf{1} - \frac{\xi}{\mathbf{E}}\right)\mathbf{d}(\mathbf{d}(\mathbf{k_i}\mathbf{A_i} - \mathbf{X})), \tag{32}$$

$$\mathbf{X} = \mathbf{V} + \omega_\mathbf{L} - \frac{\gamma^\mathbf{2}}{\chi_{\mathbf{n0}}}\mathbf{F_0^a}\mathbf{S}. \tag{33}$$

Here $E = \sqrt{(\xi^2 + \Delta^2)}$ is the unperturbed quasiparticle energy, $\xi \simeq v_f(k - k_F)$, and φ is the distribution function corresponding to global equilibrium defined by the temperature and the pressure. Spin precession in a spatially varying magnetic field changes the quasiparticle excitation energies and induces motion of the order parameter: The change in the excitation energies in spin space is given by $\delta\mathbf{E}$; the angular velocities of order parameter in spin space is $\mathbf{V}$; spatial gradients of the order parameter generate superfluid spin velocities $\mathbf{A}_i$; the local value of the equilibrium distribution becomes $\frac{\partial\varphi}{\partial E}\delta\mathbf{E}$; and $\delta\nu$ gives the actual quasiparticle distribution function in spin space. So $\delta\mu = \delta\nu - \frac{\partial\varphi}{\partial E}\delta\mathbf{E}$ is the deviation of the quasiparticle distribution function from local equilibrium.

At very low temperatures, the quasiparticle relaxation time τ_{qp} becomes dominated by collisions with the container walls. If we neglect Andreev scattering and assume only diffuse scattering at the wall, then we can estimate the ballistic quasiparticle lifetime to be

$$\tau_{\mathrm{qp}} \approx D/v_g = \frac{D}{v_F}\sqrt{\frac{\Delta_0}{k_BT}}. \tag{34}$$

The order parameter and spin velocities are connected by the relation,

$$\frac{\partial\mathbf{A}_i}{\partial t} = \frac{1}{m^*}\nabla_i\mathbf{V} - \mathbf{A}_i \times \mathbf{V}. \tag{35}$$

To calculate the dissipation function in Eq. (28) we need to determine the change in the quasiparticle distribution function, $\delta\mu$. The quasiparticle (nonequilibrium) contribution to the spin and spin current are given by

$$\delta\mathbf{S} = \sum_\mathbf{k}\left\{\frac{\xi_k}{E_k}\delta\mu + \left(1 - \frac{\xi_k}{E_k}\frac{\xi_k}{E_k}\right)\mathbf{d}(\mathbf{d}\delta\mu)\}\right\}, \tag{36}$$

$$\mathbf{J}_i = \frac{1}{2}\sum_\mathbf{k} v_{Fi}\left[\delta\mu - \left(1 - \frac{\xi}{E}\right)\mathbf{d}(\mathbf{d}\delta\mu)\right]. \tag{37}$$

We further note that in Eq. (29) we may write the time derivative of the distribution function as $\partial\delta\nu/\partial t = i\omega_p\delta\mu$ where $\omega_p \sim \omega_L$ is the precession frequency. In addition, for the low-temperature regime applicable to PPD experiments we may assume that the excitations are highly ballistic, $\omega_p\tau_{qp} \gg 1$.

A. Leggett-Takagi relaxation

Leggett-Takagi relaxation occurs when the superfluid spin component precesses at a different frequency to the local Larmor frequency.[39] In this case the normal and superfluid components of the spin move out of equilibrium with each other which generates a dissipative viscous torque.

To derive the Leggett-Takagi relaxation coefficient we consider in Eq. (29) only spatially homogeneous terms. Following the procedures developed in Refs. 35 and 36 we obtain the Leggett-Takagi dissipation function:

$$R_{\mathrm{LT}} = \tfrac{1}{2}K_{\mathrm{LT}}[(\omega_p - \omega_L)^2\sin^2\beta + \dot{\beta}^2], \tag{38}$$

where

$$K_{\mathrm{LT}} = 216\sqrt{\frac{10\pi}{3}}\frac{\chi_B}{\gamma^2}\left(\frac{k_BT}{\Delta_0}\right)^2\frac{v_F}{D}\exp\left(-\frac{\Delta_0}{k_BT}\right). \tag{39}$$

The first term on the right-hand side of Eq. (38) dominates at low temperatures since the frequency shift $\delta\omega = \omega_p - \omega_L$ is much larger than the inverse relaxation time $1/\tau \sim \dot{\beta}/\beta$. So for small deflection angles,

$$R_{\mathrm{LT}} \approx \tfrac{1}{2}K_{\mathrm{LT}}\delta\omega^2\beta^2. \tag{40}$$

Inserting this expression into Eq. (28), we find that the energy dissipation is

$$\frac{dE}{dt} = \frac{\pi^{3/2}}{2}ZR^2K_{LT}\delta\omega^2\beta_0^2. \tag{41}$$

Substituting for the energy of the spin-wave mode given by Eq. (27) gives us the following decay equation for Leggett-Takagi relaxation:

$$\frac{\chi_B}{g^2}\omega_0^2\dot{\beta}_0 = -K_{\rm LT}\delta\omega^2\beta_0. \quad (42)$$

This describes an exponential decay of the spin deflection:

$$\beta_0(t) = \beta_0(0)\exp\left(-\frac{t}{\tau_{\rm LT}}\right). \quad (43)$$

Substituting for $K_{\rm LT}$ from Eq. (39) gives us the Leggett-Takagi relaxation time:

$$\tau_{\rm LT} = \frac{1}{216}\sqrt{\frac{3}{10\pi}}\left(\frac{\Delta_0}{k_BT}\right)^2\left(\frac{\omega_0}{\delta\omega}\right)^2\frac{D}{v_F}\exp\left(\frac{\Delta_0}{k_BT}\right). \quad (44)$$

Inserting the values corresponding to our experimental conditions gives $\tau_{\rm LT} \approx 7\times10^7$ s at $T = 0.14T_C$. This is more than 5 orders of magnitude larger than the measured PPD lifetime. Although we have made this calculation specifically for the fundamental spin-wave mode, a similar result would be obtained for any similar coherently precessing structure since the important quantity which controls the relaxation is the frequency shift $\delta\omega$. We therefore conclude that Leggett-Takagi relaxation is entirely negligible at these temperatures.

B. Spin diffusion

Spin diffusion occurs wherever there is spatial inhomogeneity. Often the dynamics of the superfluid component of the spin remains coherent in spite of inhomogeneity due to the rigidity of the order parameter. The normal component, however, does not have this property, so the various kinds of inhomogeneity (e.g., from the external field, from the influence of cell walls, or from textures) generate dissipative currents.

Following the procedures used by Markelov and Mukharsky,[37] retaining just the gradient terms in Eq. (29), we obtain the diffusion dissipation function,

$$R_{\rm DF} = \tfrac{1}{2}K_{\rm DF}[\sin^2\beta(\nabla\alpha_s)^2 + (\nabla\beta)^2], \quad (45)$$

where

$$K_{\rm DF} = \frac{3}{10}\frac{\chi_B}{g^2}v_F^2\omega_0\sqrt{\frac{2\pi k_BT}{\Delta_0}}\exp\left(-\frac{\Delta_0}{k_BT}\right). \quad (46)$$

Inserting this expression into Eq. (28) we find that, for small spin deflections, the energy dissipated by the fundamental spin-wave mode is

$$\frac{dE}{dt} = -\pi^{3/2}K_{\rm DF}{\beta_0}^2\frac{R^2+2Z^2}{2Z}. \quad (47)$$

Substituting for the energy of the spin-wave mode given by Eq. (27) gives us the following decay equation for spin diffusion:

$$\frac{\chi_B}{g^2}\omega_0^2\dot{\beta}_0 = -K_{\rm DF}\frac{R^2+2Z^2}{2Z^2R^2}\beta_0. \quad (48)$$

This describes an exponential decay of the spin deflection angle,

$$\beta_0(t) = \beta_0(0)\exp\left(-\frac{t}{\tau_{\rm DF}}\right), \quad (49)$$

with a relaxation time constant of

$$\tau_{\rm DF} = \frac{10}{3}\frac{\omega_0}{v_F^2}\sqrt{\frac{\Delta_0}{2\pi k_BT}}\exp\left(\frac{\Delta_0}{k_BT}\right)\frac{Z^2R^2}{R^2+2Z^2}. \quad (50)$$

In contrast to the linear spin-wave calculation given above, the PPD decays are clearly not exponential (see Fig. 5) so it is not possible to make a direct comparison. A more accurate description must take into account the back-reaction of the precession on the orbital texture as discussed above. However, we can attempt to make a rough comparison as follows. In Fig. 7 we plot the *total* lifetime of the PPD, defined as the length of time that it remains visible on the fft (see Fig. 2). The PPD signal falls by a factor of $20 \approx \exp(3)$ during its visible decay as shown in Fig. 5. So as a crude approximation, we should compare the measured lifetimes of the PPD with $3\tau_{\rm DF}$. This is plotted as the red line in Fig. 7. The agreement with the experimental data is extremely good at intermediate temperatures, but the PPD show a longer lifetime at the higher temperatures. The data are fit far better by the black lines which have an intrinsic time constant given by Eq. (25).

C. Surface relaxation

An additional surface relaxation mechanism appears when the applied field gradient is such that the field minimum occurs close to the top of the NMR chamber so that the PPD is in partial contact with the domed end cap of the cell, shown in Fig. 1. In this case, the PPD lifetime is considerably shortened, and fits well to Eqs. (24) and (25) with a temperature-independent surface relaxation time τ_s as indicated in Fig. 7. Since the temperature range where the surface mechanism dominates is quite narrow, the data would also be consistent with τ_s having a moderate (e.g., power-law) temperature dependence.

As discussed in Ref. 40, surface relaxation can arise due to time-dependent spatial variations of the order parameter excited by spin precession close to a wall. In this case, the lifetime of precession can be estimated from general considerations. Ohmi *et al.*[40] derived an estimate for the lifetime of the spin precession in the slab geometry (perpendicular to the field):

$$\tau_s \sim \left(\frac{\chi_B}{\chi_N-\chi_B}\right)^2\frac{c}{\omega^2\xi^2}L, \quad (51)$$

where χ_N and χ_B are the susceptibilities of the normal and B phases, respectively, ξ is the superfluid coherence length, c is the spin-wave velocity (neglecting anisotropy), and L is the slab spacing. For the case of spin-wave modes in close contact with a horizontal wall, we expect a similar expression with L replaced by the vertical extent of the domain Z. Inserting the parameters relevant to our experiment conditions gives us a minimum value of the surface relation time of $\tau_s^{\rm min} \approx 0.02$ s. This is sufficiently short to account for the PPD data shown in Fig. 7. As the precessing domain is brought closer to the surface, the surface relaxation mechanism plays a greater role and the PPD lifetime is shortened dramatically.

XI. ORBITAL DYNAMICS

Due to spin orbit coupling, the spin precession generated in NMR experiments will, in general, produce a "dipole" torque

acting between the spin and orbital angular momenta. The most visible effect of this torque is to increase the frequency of the spin precession as was discussed in Sec. VI. This torque also acts on the orbital angular momentum. Damping of the orbital motion arises from scattering with thermal quasiparticle excitations. A magnetic field induces anisotropy in the quasiparticle dispersion curve: The quasiparticle energies are split by the Zeeman energy along the orbital momentum axis. The energy gap also becomes slightly anisotropic but the gap distortion only varies quadratically with field and so is negligible for the low magnetic fields typically used in NMR experiments.

Due to the anisotropy, orbital precession results in an oscillation of the quasiparticle energies and produces dissipation. The process can be conveniently described in terms of an orbital viscosity analogous to that used to describe orbital dynamics in the A phase.[41] The orbital viscosity has been calculated in Ref. 30 for both hydrodynamic and ballistic temperature regimes. The viscosity is very large at higher temperatures where the majority of experiments have been performed to date. Consequently the orbital momentum is heavily damped and orbital dynamics can be largely ignored in most NMR experiments.[30] At lower temperatures, in the ballistic regime, the orbital viscosity is roughly proportional to the quasiparticle density, becoming vanishingly small at the lowest temperatures. So in this case orbital motion may become important and one should consider coupled spin-orbit dynamics.

The equations of motion for spin-orbit dynamics are far more complicated than for spin dynamics alone.[3] Solving these for nonlinear spin-wave modes is a substantial challenge for future research. We note that for uniform textures, solutions have been found in which the orbital momentum precesses.[3] The orbital precession can either be coherent (phase locked) with the spin precession at the NMR frequency or it can be at some other frequency. Orbital precession at the NMR frequency may be very long lived[30] but since the dipole torque is relatively small it is only possible for very small amplitudes. Larger amplitudes of orbital motion are possible at lower frequencies.

XII. DISCUSSION

We have presented detailed measurements of PPDs excited by pulsed NMR at temperatures down to below 0.11 T_C. Reproducible PPDs are excited in a field minimum which can be manipulated with an applied field gradient. When located far from the end wall of the NMR chamber, the PPDs are very long lived, with lifetimes exceeding 1000 s at the lowest temperatures. We have compared the properties of the PPD with spin-wave modes excited in the potential well generated by a field minimum combined with a flare-out orbital texture. The linear spin-wave theory gives reasonable estimates for the size and the frequency shift of the PPD at late times, towards the end of its decay. However, the theory is clearly inadequate to describe the detailed time-dependent amplitude and frequency shift during the decay.

We have presented calculations for the relaxation times for the linear spin-wave modes due to the Leggett-Takagi and spin diffusion mechanisms. The Leggett-Takagi mechanism is found to be entirely redundant for these modes. Our estimates of the relaxation due to spin diffusion have a very similar magnitude to our measurements but with a slightly different temperature dependence.

As the PPD is moved towards the end wall of the cell an additional surface relaxation mechanism dominates at the lowest temperatures and the lifetimes are dramatically shortened. The additional relaxation does not significantly affect the amplitude of the PPD as a function of its frequency shift. This suggests that the amplitude-frequency response is an intrinsic property of the PPD. The surface relaxation time can be crudely estimated from general arguments, but it will be interesting to study the surface relaxation mechanism in more detail, especially in light of recent work on Majorana fermions at the surface of ^{3}He-B which may have interesting magnetic properties.[42,43] It is also interesting to note that the relaxation times at the lowest temperatures may be influenced by quantum vortex lines.[17]

A fuller theoretical description of the PPD requires a theory of nonlinear spin waves including a self-consistent description of the orbital degrees of the freedom which are crucial to the development and stability of the PPD. This is an interesting challenge for future research.

ACKNOWLEDGMENTS

We acknowledge I. E. Miller and M. G. Ward for technical support and V. B. Eltsov for useful discussions. The work was funded by the United Kingdom EPSRC and the European FP7 Programme MICROKELVIN, Project No. 228464. P.S. is grateful for support by the Centre of Low Temperature Physics, operated as the Centre of Excellence CFNT MVEP of the Slovak Academy of Sciences, by the US Steel Košice s.r.o., and by Grants No. APVV-0515-10 and No. VEGA 2/0128/12. N.S. is supported by the Leverhulme Trust Grant No. F/00125/AH.

[1] A. J. Leggett, Ann. Phys. **85**, 11 (1974).
[2] Yu. M. Bunkov and V. L. Golo, J. Low Temp. Phys. **137**, 625 (2004).
[3] S. N. Fisher and N. Suramlishvili, J. Low Temp. Phys. **141**, 111 (2005).
[4] A. S. Borovik-Romanov, Yu. M. Bunkov, V. V. Dmitriev, and Yu. M. Mukharsky, JETP Lett. **40**, 1033 (1984).
[5] Yu. M. Bunkov, in *Progress in Low Temperature Physics*, Vol. XIV, edited by W. P. Halperin (Elsevier, Amsterdam, 1995), p. 69.
[6] I. A. Fomin, JETP Lett. **40**, 1037 (1984).
[7] Yu. M. Bunkov and G. E. Volovik, Phys. Rev. Lett. **98**, 265302 (2007).
[8] G. E. Volovik, J. Low Temp. Phys. **153**, 266 (2008).
[9] A. J. Leggett and S. Takagi, Ann. Phys. **106**, 79 (1977).
[10] Yu. M. Bunkov, S. N. Fisher, A. M. Guénault, C. J. Kennedy, and G. R. Pickett, Phys. Rev. Lett. **68**, 600 (1992).

[11] Yu. M. Bunkov, O. D. Timofeevskaya, and G. E. Volovik, Phys. Rev. Lett. **73**, 1817 (1994).
[12] P. Skyba, R. Harakály, L. Lokner, and A. Feher, Phys. Rev. Lett. **75**, 477 (1995).
[13] Yu. M. Bunkov, V. S. L'vov, and G. E. Volovik, JETP Lett. **84**, 349 (2006).
[14] D. A. Geller and D. M. Lee, Phys. Rev. Lett. **85**, 1032 (2000).
[15] Yu. M. Bunkov, J. Low Temp. Phys. **135**, 337 (2004).
[16] Yu. M. Bunkov, S. N. Fisher, A. M. Guénault, and G. R. Pickett, Phys. Rev. Lett. **69**, 3092 (1992).
[17] S. Autti, Yu. M. Bunkov, V. B. Eltsov, P. J. Heikkinen, J. J. Hosio, P. Hunger, M. Krusius, and G. E. Volovik, Phys. Rev. Lett. **108**, 145303 (2012).
[18] S. N. Fisher, A. M. Guénault, A. J. Hale, G. R. Pickett, P. A. Reeves, and G. Tvalashvili, J. Low Temp. Phys. **121**, 303 (2000).
[19] D. J. Cousins, S. N. Fisher, A. I. Gregory, G. R. Pickett, and N. S. Shaw, Phys. Rev. Lett. **82**, 4484 (1999).
[20] S. N. Fisher, A. M. Guénault, G. R. Pickett, and P. Skyba, Physica B **329–333**, 80 (2003).
[21] D. I. Bradley, D. O. Clubb, S. N. Fisher, A. M. Guénault, C. J. Matthews, G. R. Pickett, and P. Skyba, J. Low Temp. Phys. **134**, 351 (2004).
[22] S. N. Fisher, A. M. Guénault, C. J. Matthews, G. R. Pickett, P. Skyba, and K. L. Zaki, J. Low Temp. Phys. **138**, 777 (2005).
[23] V. B. Eltsov, R. de Graaf, M. Krusius, and D. E. Zmeev, J. Low Temp. Phys. **162**, 212 (2011).
[24] G. R. Pickett and S. N. Fisher, Physica B **329**, 75 (2003).
[25] D. I. Bradley, S. N. Fisher, A. M. Guénault, R. P. Haley, and G. R. Pickett, J. Low Temp. Phys. **135**, 385 (2004).
[26] D. J. Cousins, S. N. Fisher, A. M. Guénault, R. P. Haley, I. E. Miller, G. R. Pickett, G. N. Plenderleith, P. Skyba, P. Y. A. Thibault, and M. G. Ward, J. Low Temp. Phys. **114**, 547 (1999).
[27] S. N. Fisher, A. M. Guénault, C. J. Kennedy, and G. R. Pickett, Phys. Rev. Lett. **63**, 2566 (1989).
[28] C. Bäuerle, Yu. M. Bunkov, S. N. Fisher, and H. Godfrin, Phys. Rev. B **57**, 14381 (1998).
[29] M. Kupka and P. Skyba, Phys. Lett. A **317**, 324 (2003).
[30] S. N. Fisher and N. Suramlishvili, J. Low Temp. Phys. **138**, 771 (2005).
[31] G. Kharadze and G. Vachnadze, JETP Lett. **56**, 458 (1992).
[32] D. D. Osheroff, Physica B **90**, 20 (1977).
[33] D. S. Greywall, Phys. Rev. B **33**, 7520 (1986).
[34] D. Candela, D. O. Edwards, A. Heff, N. Masuhara, Y. Oda, and D. S. Sherrill, Phys. Rev. Lett. **61**, 420 (1988).
[35] A. V. Markelov, Sov. Phys. JETP **64**, 1218 (1986).
[36] A. V. Markelov, JETP Lett. **62**, 668 (1995).
[37] A. V. Markelov and Yu. M. Mukharsky, Physica B **178**, 202 (1992).
[38] R. Combescot, Phys. Rev. B **13**, 126 (1976).
[39] A. J. Leggett and S. Takagi, Ann. Phys. **110**, 353 (1978).
[40] T. Ohmi, M. Tsubota, and T. Tsuneto, Japanese Journal of Applied Physics, supplement 26-3, 169 (1987).
[41] M. C. Cross and P. W. Anderson, *Proceedings of the 14th International Conference on Low Temperature Physics LT-14*, Part I, edited by M. Krusius and M. Vuorio (North-Holland, Amsterdam, 1975), p. 19.
[42] Y. Nagato, S. Higashitani, and K. Nagai, J. Phys. Soc. Jpn. **78**, 123603 (2009).
[43] Suk Bum Chung and Shou-Cheng Zhang, Phys. Rev. Lett. **103**, 235301 (2009).